Hindawi Publishing Corporation
Journal of Nanotechnology
Volume 2009, Article ID 176517, 10 pages
doi:10.1155/2009/176517

Review Article

Structural and Electrochemical Characterization of Pure $LiFePO_4$ and Nanocomposite C-$LiFePO_4$ Cathodes for Lithium Ion Rechargeable Batteries

Arun Kumar,[1] R. Thomas,[1] N. K. Karan,[1] J. J. Saavedra-Arias,[1] M. K. Singh,[2] S. B. Majumder,[3] M. S. Tomar,[4] and R. S. Katiyar[1]

[1] *Department of Physics and Institute for Functional Nanomaterials, University of Puerto Rico, San Juan, PR 00931-3343, USA*
[2] *Centre of Material Sciences, University of Allahabad, Allahabad 211002, India*
[3] *Materials Science Center, Indian Institute of Technology, Kharagpur 721302, India*
[4] *Department of Physics, University of Puerto Rico, Mayaguez, PR 00680-9016, USA*

Correspondence should be addressed to R. Thomas, etreji@yahoo.com and R. S. Katiyar, rkatiyar@uprrp.edu

Received 14 March 2009; Revised 12 August 2009; Accepted 2 December 2009

Recommended by Ram B. Gupta

Pure lithium iron phosphate ($LiFePO_4$) and carbon-coated $LiFePO_4$ (C-$LiFePO_4$) cathode materials were synthesized for Li-ion batteries. Structural and electrochemical properties of these materials were compared. X-ray diffraction revealed orthorhombic olivine structure. Micro-Raman scattering analysis indicates amorphous carbon, and TEM micrographs show carbon coating on $LiFePO_4$ particles. Ex situ Raman spectrum of C-$LiFePO_4$ at various stages of charging and discharging showed reversibility upon electrochemical cycling. The cyclic voltammograms of $LiFePO_4$ and C-$LiFePO_4$ showed only a pair of peaks corresponding to the anodic and cathodic reactions. The first discharge capacities were 63, 43, and 13 mAh/g for C/5, C/3, and C/2, respectively for $LiFePO_4$ where as in case of C-$LiFePO_4$ that were 163, 144, 118, and 70 mAh/g for C/5, C/3, C/2, and 1C, respectively. The capacity retention of pure $LiFePO_4$ was 69% after 25 cycles where as that of C-$LiFePO_4$ was around 97% after 50 cycles. These results indicate that the capacity and the rate capability improved significantly upon carbon coating.

Copyright © 2009 Arun Kumar et al. This is an open access article distributed under the Creative Commons Attribution License, which permits unrestricted use, distribution, and reproduction in any medium, provided the original work is properly cited.

1. Introduction

Lithium iron phosphate ($LiFePO_4$) is under intense investigation since its introduction in 1997 as a possible cathode material for Li-ion rechargeable batteries [1]. $LiFePO_4$ belongs to the olivine type compound exhibiting a theoretical capacity of ~170 mAh/g and a flat charge/discharge profile at ~3.4 V versus Li/Li^{1+}. Additionally, the cost effectiveness, environmental and safety returns (high abuse tolerance), thermal stability at fully charged state, and reasonably good cycleability have made $LiFePO_4$ as one of the most attractive cathode materials for rechargeable Li-ion batteries. However, for successful commercial acceptance several material related issues, which can be grouped into three categories, should be addressed. (i) *Synthesis of phase pure olivine lithium iron phosphate at relatively low processing temperatures*. Various synthesis routes have been adopted to synthesize phase pure lithium iron phosphate such as solid-state synthesis [2, 3], sol-gel [4, 5], microemulsion synthesis [6], hydrothermal synthesis [7, 8], and so forth. The reported research [2–8] indicates that it is important to select proper precursor materials as well as optimize process parameters to keep iron in its +2 valence state to suppress the formation of impurity phase such as Li_3PO_4. Use of carbon with the precursor materials and calcinations at inert ambient has been found to be useful to retard the iron oxidation and thereby limiting the formation of impurity phase. (ii) *The poor ionic as well as electronic conductivities of $LiFePO_4$ materials* [9]. In several reports, carbon coating improved the Li-ion kinetics in $LiFePO_4$ cathode materials [2, 5, 7, 10]. In contrast to this popular belief, it is also argued that the effect of carbon coating is marginal [11]. However, $LiFePO_4$ community now reached a consensus and believes that carbon coating is beneficial in improving the electrochemical performances of $LiFePO_4$. Efforts have also been undertaken to eliminate carbon

coating with other metal dispersion (namely, copper or silver) [12, 13] or conducting organic materials (namely, polypyrole) [14]. Initially, it was believed that the intrinsic electronic conductivity of $LiFePO_4$ could be improved by aliovalent dopants substitution and is now understood that it was an artifact due to the presence of carbon in the precursor, and also of metallic Fe2P impurities [15–18]. (iii) *Control on the particle size in the nanoregime along with a narrow particle size distribution of the synthesized $LiFePO_4$ cathode materials*. Li^+ has slow diffusivity in $LiFePO_4$ (D_{Li} ~10^{-14}–10^{-16} cm^2/s) compared to the widely used layered $LiCoO_2$ ((D_{Li} ~10^{-12}–10^{-13} cm^2/s) [19–21]. As a result, only ~60%–70% of the capacity could be obtained for the original $LiFePO_4$ in the early works, and its capacity decreases remarkably at larger current density. Hence, maintaining particle size in nano-regime (to ensure shorter diffusion length for realizing maximum (de)intercalation within the stipulated time) has been reported to improve discharge capacity as well as rate capability [22]. Here again, addition of carbon is beneficial in suppressing the particle growth during high-temperature calcinations. The above discussion on the three material related issues of $LiFePO_4$ for cathode application clearly suggests that addition of carbon could be beneficial in addressing all three issues and yielding phase-pure olivine, enhancing its electronic conductivity and retarding the particle growth.

Despite aforementioned improvements, the nature of the morphology of C-$LiFePO_4$ composite is yet to be properly understood. Earlier, it was not clear whether carbon should form a thin coating on $LiFePO_4$ particles or point contacts between particles to have beneficial effect on the discharge capacity and the rate capability. Research efforts have also been directed to elucidate whether crystalline or amorphous carbon is beneficial for the targeted electrochemical properties. At present it is believed that an amorphous thin coat insures point contact [23]. The process complexities, as outlined above, are reflected in the electrochemical properties of C-$LiFePO_4$ cathode materials. Hence, a comparative study of pure $LiFePO_4$ and composite C-$LiFePO_4$ in terms of structure and electrochemical properties may be of importance to understand the role carbon in $LiFePO_4$. The details of the electrochemical data from some of the recent literature report are summarized in Table 1. It is seen from Table 1 that the scattering of the data is thought to be stemmed out mostly from one (or more) of the three factors mentioned above. The routes and conditions used to synthesize $LiFePO_4$ have, in general, profound influence on its electrochemical properties, where highest discharge capacity obtained was around 163 mAh/g with C/10 rate [4]. However, in terms of rate capability best results reported so far are 120 mAh/g with 10 C [24]. In view of the above discussion, there is a compelling need for optimization of the synthesis process to obtain phase pure nanocrystalline C-$LiFePO_4$ composite cathode materials for its reliable cathode applications in Li-ion batteries. Also, the knowledge about the lattice dynamics is essential for understanding the phase transformation during Li-ion (de)intercalation of C-$LiFePO_4$ and Raman spectroscopy is a valuable technique for such studies [25–29]. In the present case, a solid-state route under nitrogen ambient has been adopted to synthesize pure $LiFePO_4$ and C-$LiFePO_4$ composite cathodes at a relatively low temperature and their structural and electrochemical properties have been studied and compared. Moreover, the Raman spectra of C-$LiFePO_4$ at various stages of charging and discharging have been taken to study the structural reversibility.

2. Experimental Details

Stoichiometric amount of lithium carbonate (Li_2CO_3 (99.999%, Alfa Aeasar)), iron oxalate ($FeC_2O_4 \cdot 2H_2O$ (99.999%, Alfa Aeasar)), and ammonium dihydrogen phosphate (99.995% Alfa Aeaser) were used as precursor materials to prepare $LiFePO_4$ pure and C-$LiFePO_4$ composite cathode materials. High-energy balling system was used for the synthesis of $LiFePO_4$ and C-$LiFePO_4$ powders. These reagents mixtures were first ball milled for 10–18 hours in acetone media and vacuum dried in the furnace at 150°C to predecompose the oxalate and phosphate. The obtained powder was grinded in the glove box under argon atmosphere to suppress the oxidation ferrous iron (Fe^{2+}) to ferric iron (Fe^{3+}) and subsequently fired at 400°C for 5 hours in flowing nitrogen to ensure complete organic removal. After this step, the powder was divided into two halves, and one half was mixed with 8 wt% carbon black and again ball milled without any solvent. Then the two batches of the powders (with and without carbon) were calcined in the temperature range of 500–750°C for 4 hours in flowing N_2 atmosphere to obtain pure $LiFePO_4$ (without carbon) and C-$LiFePO_4$ (composite) cathode materials.

The phase formation behavior of the synthesized powders was investigated using X-ray diffraction (XRD, Siemens D5000), diffractometer with Cu Kα radiation (λ = 1.54056 Å). The XRD data were collected in the range 10–80° with a step of 0.02° and a count time of 1 second per step. XRD spectra were refined by Reitveld method using the Fullprof package to identify the structural change of pristine samples [31]. The morphology of the synthesized powder was investigated using a scanning electron microscopy (SEM) and transmission electron microscopy (TEM, Carl Zeiss Leo Omega 922 at 200 KeV). The nature of carbon coating on the pristine lithium iron phosphate was characterized using TEM in conjunction with the Raman scattering measurements (T64000 spectrometer equipped with a triple-grating monochromator and a Coherent Innova 90C Ar^+-laser at 514.5 nm).

In order to evaluate the electrochemical characteristics of the synthesized powder, the working electrode (cathode) was prepared as follows: first a slurry was made by mixing 80 wt% active material (C-$LiFePO_4$), 12 wt% binder (polyvinylidine fluoride (PVDF, Alfa Aesar)), and 8 wt% carbon black in a solvent N-methyl pyrrolidone. The slurry was coated on aluminum foil current collector and dried in an oven at 60°C for 12 hrs. The dried electrode was used as cathode to fabricate coin cell (CR 2032) which was comprised of lithium foil as an anode and $LiPF_6$ (1 M) (in a mixture of ethylene carbonate and dimethyl carbonate in 1 : 1 ratio) as an electrolyte. The fabrication of coin cell assembly was carried out in Ar atmosphere inside a glove box. A computer

Table 1: Electrochemical properties of lithium iron phosphate cathode.

Synthesis route	C coating/C added (wt%)	Capacity (mAh/g)/(C rate)	Particle size (nm)
High-energy ball mill [3]	No/No	160 (C/10) 104 (3C)	
Microemulsion synthesis [6]	Yes/5	163 (C/10) 130 (2C)	90–200 nm
Spray drying [19]	Yes/5.1	139.4 (C/5) 137.2 (1C) 133.5 (5C) 127.3 (10C)	80–300 nm
Solution route [4, 16]	Yes/15	160 (C/10) 142 (C) 120 (5C)	100–200 nm
Solution route [24]	Yes/12	160 (C/2) 150 (1C) 135 (5C) 120 (10C)	174 nm
Hydrothermal process [30]	Yes/15	140 (C/10) 125 (C/2) 110 (1C)	0.5 μm
This work	No/8	63 (C/5) 43 (C/3) 13 (C/2)	200 nm
This work	Yes/8	163 (C/5) 144 (C/3) 118 (C/2) 70 (1C)	200 nm

controlled potentiostat-galvanostat system (Solatron battery-testing unit 1470E) was utilized for electrochemical measurements. The cyclic voltammograms (CV) were recorded at various voltage scan rate ranging 0.1–0.5 mVs^{-1} with a cut-off limit 2.5–4.3 V versus Li/Li^+. The CV data were analyzed to estimate the diffusion coefficient of Li^+ at room temperature. The charge discharge measurements were performed with various current densities.

3. Results and Discussion

3.1. Structure and Morphology. X-ray diffraction patterns of pure $LiFePO_4$ and of C-$LiFePO_4$ materials (calcined at 700°C for 4 h in nitrogen ambient) are shown in Figure 1(a). All the major reflections in the XRD pattern were indexed based on orthorhombic olivine structure (space group Pnma). Some additional peaks (marked by arrows, corresponding to the crystalline impurity phases) were also observed in the XRD pattern of $LiFePO_4$. These peaks at 27°, 31°, and 33° are probably due to $Li_3Fe_2(PO_4)_3$. In some of the reported works it is argued that the deficiency of ferrous iron in oxalate resulted detectable amount of $Li_3Fe_2(PO_4)_3$ phase [32]. However, XRD pattern of C-$LiFePO_4$ (8 wt% C) clearly shows the ideal orthorhombic olivine structure (JCPDS card no. 40–1499) without any impurity phase compared to pure $LiFePO_4$ synthesized without carbon mixing. In $Li_3Fe_2(PO_4)_3$ iron present in the Fe^{3+} oxidation state where as in $LiFePO_4$ it is present in the Fe^{2+} oxidation state. Therefore, we speculate carbon mixing ensured reduction of Fe^{3+} to Fe^{2+} or suppress the formation of trivalent Fe ion in an oxygen deficient atmosphere (like N_2 used in the present case), resulting in the formation of single phase orthorhombic $LiFePO_4$ [33]. The calculated XRD pattern based on Reitveld fit along with the experimental pattern are also shown in Figure 1(b). Excellent match between the experimental and calculated XRD patterns is clearly seen in Figure 1(b). The calculated lattice parameters were a = 10.328 (1) Å, b = 6.0084 (6), and c = 4.6991 (6) Å with agreement parameters R_p = 2.573% and R_{wp} = 3.33%. The refined parameters match quite well with the existing literature report in carbon-coated $LiFePO_4$ particles [34].

Figure 2 shows the scanning electron micrographs (SEMs) of pure $LiFePO_4$ and C-$LiFePO_4$ powders (calcined at 700°C in nitrogen ambient). In the case of pure $LiFePO_4$ flake-like particles with large size distribution (200 nm to 1 μm) were observed. However, in the case of C-$LiFePO_4$,

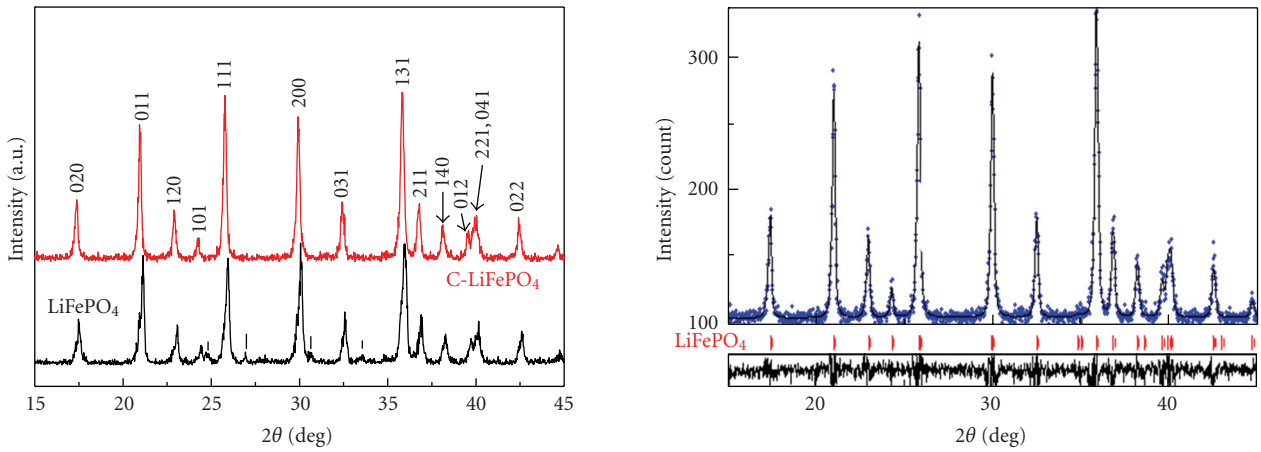

Figure 1: XRD patterns of $LiFePO_4$ material (a) with and without carbon and (b) Rietveld refinement of C-$LiFePO_4$ composite material.

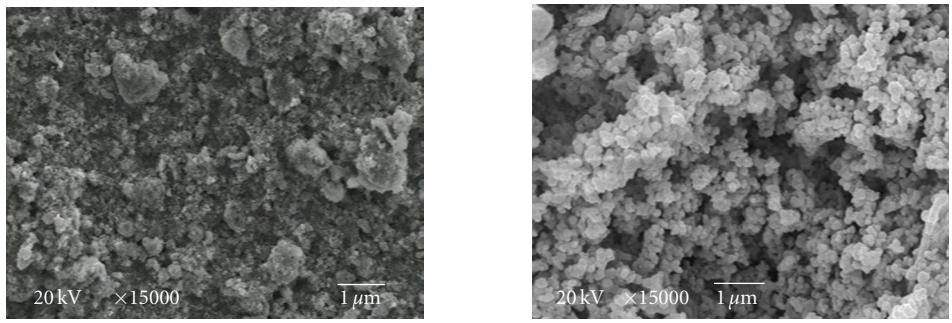

Figure 2: SEM images of $LiFePO_4$: (a) without carbon; (b) with carbon source.

particles were more uniform with narrow size distribution (80 to 200 nm). Hence, the carbon, as an additive, inhibits the particle growth (even when lithium iron phosphate is calcined at relatively higher calcinations temperature) yielding a homogeneous particle size distribution with an average particle size of ~200 nm. To understand the effect of carbon, the C-$LiFePO_4$ composite powder was characterized by TEM and Figures 3(a)–3(c) show the results. From the TEM micrograph it is apparent that the particles form agglomeration in most of the region (Figure 3(a)); however, in selected region separated particle with size < 200 nm is observed. The energy dispersive spectrometry results of the carbon mapping on the C-$LiFePO_4$ particles (Figure 3(b)) showed that carbon was evenly distributed on the composite particles.

Raman scattering is quite sensitive to changes in the local lattice distortions and change in polarizibility arising due to delithiation process in lithium-based rechargeable batteries. The C-$LiFePO_4$ is characterized by orthorhombic (triphylite) structure with the space group (Pmnb) [27]. The 34 Raman active modes can be classified as follows [27]: $\Gamma = 11A_g + 7B_{1g} + 11B_{2g} + 7B_{3g}$. The Raman scattering data of C-$LiFePO_4$ during the electrochemical cycling (half charge(HC), full charge(FC), half discharge(HC), and full discharge(FD)) were obtained by employing normal backscattering geometry and the results are presented in Figure 4(a). We observed intense Raman modes at 216, 278, 390, 441, 950, 992, 1045, and comparatively less intense Raman mode at 429 560, 626 cm^{-1} in pristine C-$LiFePO_4$, which are comparable to the earlier reported Raman spectra of C-$LiFePO_4$ with the same orthorhombic symmetry [27–29]. The Raman mode at 441 cm^{-1} is the bending mode involving O–P–O symmetry mode and disappeared in full charge Raman spectrum (i.e., believed to be pure $FePO_4$) during Li deintercalation suggest that it is highly sensitive to the local lithium environment. The Raman mode at 441 cm^{-1} was not observed in $FePO_4$; hence it also reveals that the C-$LiFePO_4$ completely transformed into C-$FePO_4$ at full charging stage [29]. The Raman modes in the range of 900 to 1150 cm^{-1} (see Figure 4(b)) are due to the stretching mode of PO_4^{3-} unit and involve symmetric and asymmetric of P–O bonds. These Raman modes show a small red and blue frequency shift during the charging and discharging process could be due to change in bond length and due to this Raman shift the A_g Raman mode at 950 cm^{-1} appears nicely in full discharge spectrum as shown

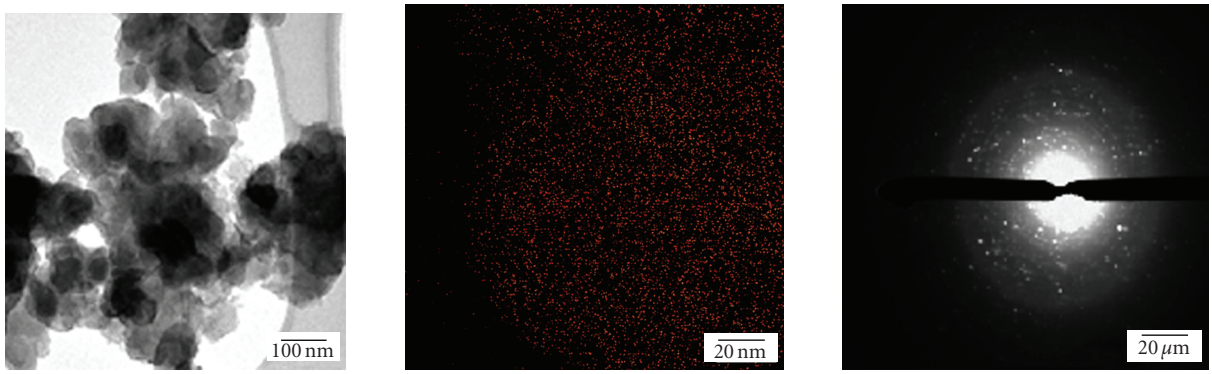

Figure 3: Transmission electron micrograph showing (a) particle morphology and size distribution of C-$LiFePO_4$ composite material, (b) C Elemental mapping of $LiFePO_4$, and (c) selected area electro diffraction (SAED) pattern of C-$LiFePO_4$.

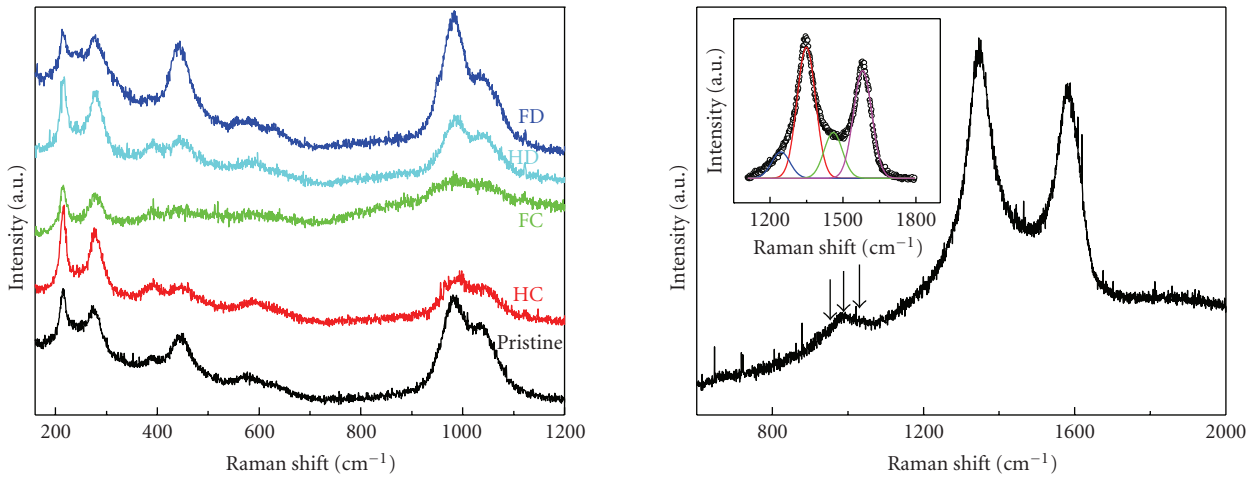

Figure 4: (a) Raman spectra of C- $LiFePO_4$ powder at various stages of charge – discharge process (half charge(HC), full charge(FC), half discharge(HC) and full discharge(FD)) in frequency range 150 to 1200 cm^{-1}. (b) Raman spectra of C- $LiFePO_4$ powder in the frequency range 600 to 1800 cm^{-1} (inset presents resolved Raman spectra of the residual carbon using Gaussian distribution function).

in inset of Figure 4(a). These Raman modes also show a systemic change in Raman intensity with electrochemical cycling process; that is, Raman intensity of all the PO_4^{3-} generated optical modes decreases during charging process and vice versa during discharging process it reveals that the polarizable derivatives of the C-$LiFePO_4$ change during Li deintercalation because the vibrational potential energy of the PO_4^{3-} is affected by change in Li/Li^+ and Fe^{2+}/Fe^{3+} ions during the Li deintercalation/intercalation. From the Raman results, structural stability and electrochemical reversibility of C-$LiFePO_4$ was observed clearly during the charging and discharging process.

In order to get further insight on the nature of carbon coating, micro-Raman scattering measurements were done on the pristine C-$LiFePO_4$ (calcined at 700°C) and the result is shown in (Figure 4(b)). The weak Raman modes (marked by small arrows) before 850 cm^{-1} have been discussed previously. The two prominent modes at ~1345 and 1587 cm^{-1} are the fingerprints of amorphous carbon [35–37]. The mode at ~1587 cm^{-1} is assigned to sp^2 graphite like (G band) and the mode at ~1345 cm^{-1} is assigned to sp^3 type amorphous carbonaceous material (D band) [38]. It is apparent from the figure that the intensity ratio between the carbon and PO_4 bands is very high. The large intensity ratio may be due to uniform carbon coating on lithium iron phosphate particles. Interestingly, in a recent report, Nakamura et al. [38] have correlated the measured resistivity of $LiFePO_4$ with the integrated intensity ratio of carbon bands to PO_4 band. Indeed a marked drop in resistivity was reported with an increase in the intensity ratio of up to 300. To resolve the Raman spectra of the residual carbon, bands were deconvoluted using Gaussian distribution function. As shown in the inset of Figure 4(b), four Raman modes yielded satisfactory fit with minimum fitting error. The mode at 1244 cm^{-1} may be related to short range vibrations of sp^3 coordinated carbons. The mode at 1460 cm^{-1} might have

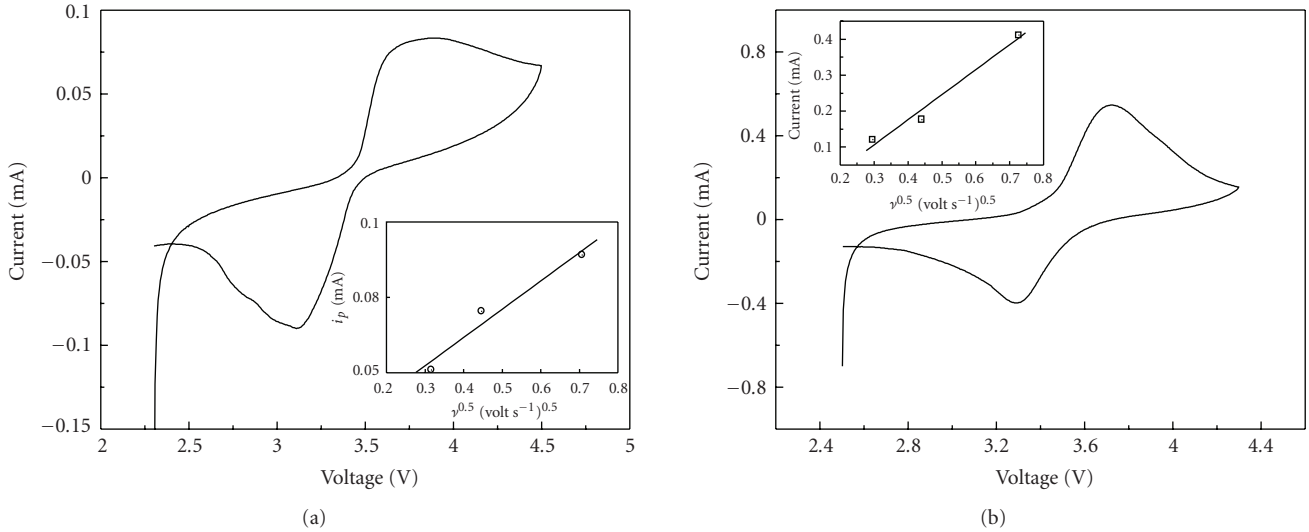

Figure 5: The CV profile of the different sample: (a) without carbon and (b) with carbon at the scan rate of 0.5 mVs^{-1}.

been arisen from Li_2CO_3 as Li_2CO_3 has Raman active modes at 700, 710, 1100, and 1480 cm^{-1} [39]. From structural and morphological results it is apparent that carbon addition imparts carbothermal reduction of Fe^{3+} ions and thereby prevents the formation of undesirable iron (II, III) pyrophosphates or phosphate impurity phases. Also, adding carbon to the starting ingredients for the synthesis effectively retards the particle growth [40] and this processing ensured uniform carbon coating on lithium iron phosphate particles.

3.2. Electrochemical Properties. For the potential battery applications of the $LiFePO_4$ and C-$LiFePO_4$ cyclic voltammograms (CV) was used to evaluate the electrochemical performance. Figure 5 shows the cyclic voltammograms (CV) of $LiFePO_4$ and C-$LiFePO_4$. In both cases, the separation between cathodic (Li^+ intercalation into the cathode) and anodic (Li^+ deintercalation from the cathode) peaks and the peak height gradually reduced as the scan rate increased. Various researchers have also reported this kind of observation [41, 42]. If the electron transfer processes were "slow" (relative to the voltage scan rate), this kind of behavior is observed in the electrochemical systems, and low electronic conductivity of $LiFePO_4$ may be responsible for the slow electron transfer. It is seen from Figure 5(a) that the anodic/cathodic peaks of pure $LiFePO_4$ are located at ~3.9 V/3.1 V at the scan rate of 0.5 mVs^{-1} and the I_p of the redox peaks is around 8×10^{-5} A. The big separation between redox peaks (ΔV) of ~0.70 V indicates that the electrochemical behavior is controlled by the diffusion step. From Figure 5(b), it can be seen that the Ip of C-$LiFePO_4$ composite material increased to 5.5×10^{-4} A for the same scan rate. Meanwhile, the ΔV between redox peaks were reduced 0.5 V in composite C-$LiFePO_4$ under the same scan rate. The high current level in composite cathode compared to pure $LiFePO_4$ for the same scan rate is presumably due to higher electronic conductivity as the result of carbon coating, which might be advantageous for obtaining higher capacity at high C-rate (will be discussed later). Also, for C-$LiFePO_4$ composite cathode, well-developed CV loop confirms that the kinetics of lithium intercalation and deintercalation is markedly improved by the amorphous carbon coating compared to pure $LiFePO_4$.

Now it will be interesting to compare the chemical diffusion coefficient of Li into the electrode material as this mainly determines achievable capacity and rapid diffusion of ions, which is of practical importance for fast storage/drainage of energy. The electrochemical methods, like, Impedance Spectroscopy [43, 44], Galvanostatic Intermittent Titration Technique (GITT) [45], and cyclic voltammetry (CV) [46], are widely used to measure the chemical diffusion coefficients. However, calculation of the diffusion coefficient of Li-ion from CV [47–50] is more popular as this technique is straightforward and relatively uncomplicated. In this method, the voltammetric peaks have been used to calculate the chemical diffusion coefficient of Li^+ as described by the Randles–Sevcik equation (for semi-infinite diffusion):

$$i_p = 2.69 \times 10^5 n^{3/2} C_0^b A D_{Li}^{1/2} \nu^{1/2}, \quad (1)$$

where i_p the peak current value, n is the number of electrons involved in the reaction of the redox couple (for Li^{1+} it is 1), C_0^b is the concentration (0.0228 mol/cm^3 in the present case), A is the effective working electrode area (0.423 cm^2 in the present case), ν is the rate at which the potential is swept (V/s), and D_{Li} is the diffusion coefficient (cm^2/s) of Li^+. In (1), peak current (i_p) is proportional to $v^{1/2}$. Inset of Figures 5(a) and 5(b) shows the variation i_p with square root of scan rate, and the observed linearity is consistent with the semi-infinite diffusion-controlled behavior for the range of scan-rate used [48]. From the slope of the linear fit, the calculated Li-ion chemical diffusion coefficients were 1.28×10^{-15} cm^{2}s^{-1} and 7.13×10^{-14} cm^{2}s^{-1}, respectively, for pure $LiFePO_4$ and C-$LiFePO_4$ cathodes. The order of diffusion coefficient matches well with the reported values [19, 21]. Again, the diffusion coefficient of lithium ion

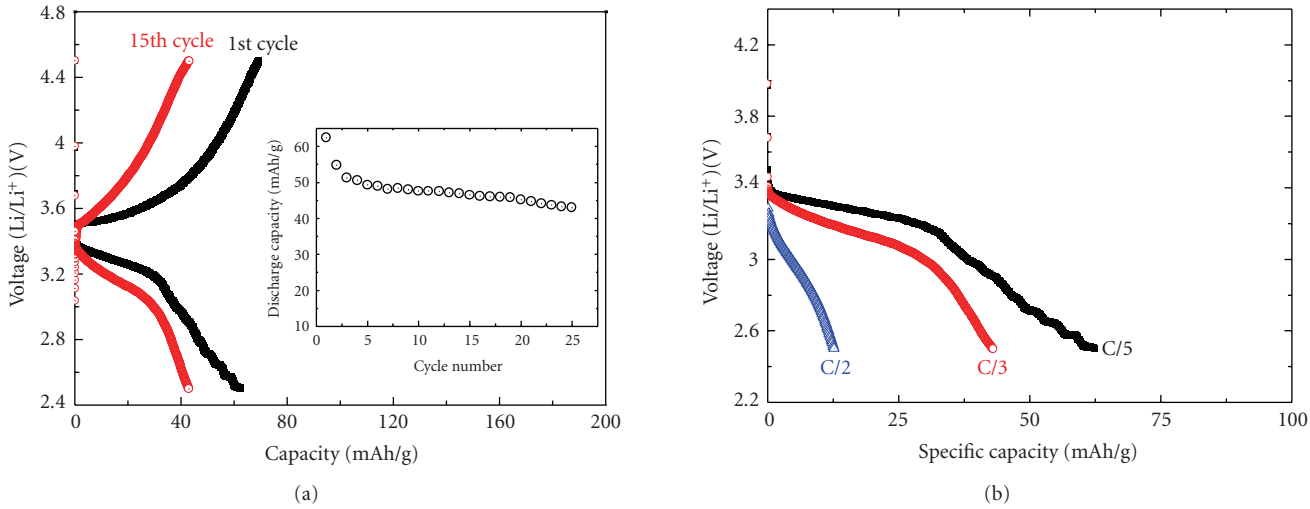

FIGURE 6: (a) Charge/discharge profile of $LiFePO_4$ sample without carbon source and inset discharge up to 25 cycles; (b) discharge profile of $LiFePO_4$ sample with carbon source at discharge rate of C/5, C/3, and C/2.

increases markedly after mixing with carbon and hence high capacity is expected for the composite cathode under the same charge/discharge conditions. Similar trend was also reported recently [20]. The lower D_{Li} in the case of untreated $LiFePO_4$ may be due to the presence of impurity phases, as diffusion of Li^+ will be hindered near the region where two phases coexisted due to the phase boundary movement [21].

Coin cells using $LiFePO_4$ and C-$LiFePO_4$ cathode and lithium anode were galvanostatically charged and discharged between 2.3 and 4.3 V at room temperature. Figure 6(a) exhibits charge and discharge profiles for 1st and 15th cycles for pure $LiFePO_4$ at a rate of C/5. The electrode material delivers a first cycle charge and discharge capacity of 70 and 63 $mAhg^{-1}$, respectively, and has a short plateau near 3.4 V. The discharge capacity reduced to 42 $mAhg^{-1}$ after 25 cycles (inset of Figure 6(a)), which corresponds to 69% capacity retention. The rate capability of pure $LiFePO_4$ was also studied and the results are shown in Figure 6(b). The obtained discharge capacities were ~63, 43, and 13 mAh/g for C/5, C/3, and C/2 rates, respectively. The poor charge-discharge characteristics of untreated $LiFePO_4$ are due to the low electronic conductivity and hindrances to the Li-diffusion into the cathode (lower D_{Li}) as mentioned earlier. Figure 7(a) shows charge and discharge profiles for 1st and 50th cycles for C-$LiFePO_4$ at a rate of C/5. The electrode delivers a discharge capacity of ~163 $mAhg^{-1}$ in the first cycle, which is significantly higher than the pure $LiFePO_4$. Recent literature reports (see Table 1) reveal that C-$LiFePO_4$ material can not only supply large capacity under high-rate but also excellent capacity retention. In the present case, at a rate of C/5, (inset of Figure 7(a)) capacity retention up to ~97% is achieved after 50 charge discharge cycles. The capacity retention is one of the best as compared to C-$LiFePO_4$ composite cathodes reported by the others. The C-$LiFePO_4$ cathodes were also characterized in terms of their rate capability and the results are shown in Figure 7(b) for C/5, C/3, C/2, and 1C rates. The obtained discharge capacities were 163, 144, 118, and 70 mAh/g, respectively, for C/5, C/3, C/2 and 1C rates. In the case of carbon-coated $LiFePO_4$ decreasing D/G intensity ratio is related to the carbon disorder and the width of the Raman line is related to the degree of carbon disorder. In the present case D/G intensity ration was higher than that reported by Julien et al. [35], and hence degree of carbon disorder (amorphous nature) is lower and conductivity may be lower due to this effect. This can be the reason for the reduced capacity at high C-rate; in the present case it may be due to the slow diffusion coefficient of Li ion in $LiFePO_4$ cathode material and lower conductivity of the conductive carbon coating.

Thus, carbon-treated $LiFePO_4$ proved to be far better compared to untreated $LiFePO_4$ as it enhanced lithium-ion transport and electronic conductivity. However, the reduction in the discharge capacity (our case) with increase in the C-rate is a concern and mainly depends on the electronic conductivity and Li-ion diffusion. Solid-state diffusion often limits the utilization and rate capability of electrode materials in a lithium-ion battery, especially at high charge/discharge rates. When the fluxes of Li^+ insertion or extraction exceed the diffusion-limited rate of Li^+ transport within the bulk phase of an electrode, concentration polarization occurs. Further, large volume changes associated with Li^+ insertion or extraction could induce stresses in bulk electrodes, potentially leading to mechanical failure. Reducing the particle size of electrodes material ensures high surface to-volume ratio, which would increase the electrochemical reaction surface and suppress the mechanical stress. To get an idea regarding the particle size effect on the rate capability, the relation between diffusion time constant (τ) and characteristic diffusion length ($L_{Li,max}$) described by Levi et al. in a recent report [51] can be used:

$$L_{Li,max} = \sqrt{\tau D_{Li}}. \quad (2)$$

Therefore, the time for intercalation varies as square of the length scale and is faster for smaller particles. In this

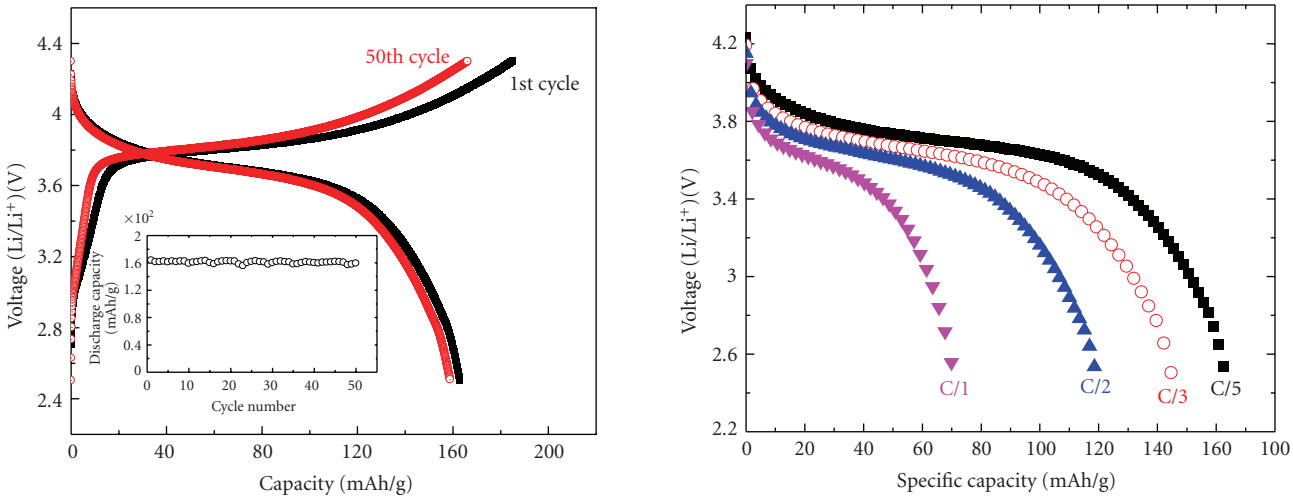

FIGURE 7: (a) Charge / discharge profile of $LiFePO_4$ sample with carbon source and inset discharge up to 50 cycles; (b) discharge profile of $LiFePO_4$ sample with carbon source at discharge rate of C/5, C/3, C/2, and 1C.

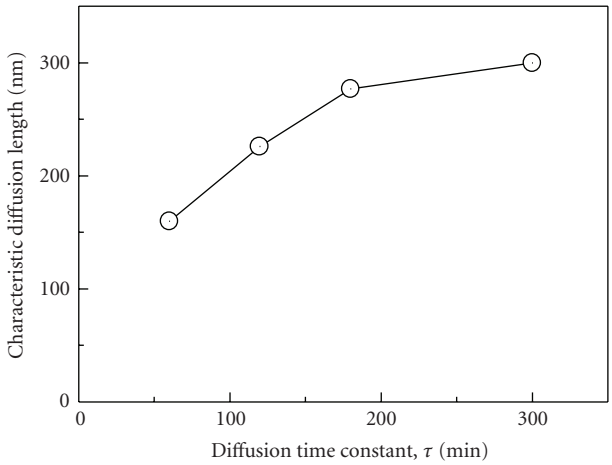

FIGURE 8: Variation of Characteristic diffusion length with C-rate.

regard, optimal Li insertion could be achieved when (decided by chosen current density of discharge) $L_{Li,max}$ is comparable or larger than the particle size of the cathode material. Alternately, if the τ is higher than charging or discharging time, one can obtain maximum limit of capacity for a given temperature. Hence (2) can be used as a measure to design the particle size for obtaining maximum capacity at high C-rate (fast charging and discharging) for materials with low ionic diffusion as in the case of $LiFePO_4$. As mentioned earlier, the average diffusion coefficient estimated from the CV data is $\sim 7.13 \times 10^{-14}\,cm^2s^{-1}$. As a rough estimation, by taking this value of D_{Li} and the discharge time we have calculated $L_{Li,max}$. The characteristic diffusion length decreased with C-rate (see Figure 8) and the values of D_{Li} were 160 nm, 226 nm, 277 nm, and 357 nm for 1C, C/2, C/3, and C/5 rate, respectively. It can be seen that for smaller diffusion time (faster charging/discharging) the dependence on the $L_{Li,max}$ is stronger. The estimated values are indicative of obtaining better electrochemical performance at higher current rate, with reduced particle size. As envisaged from SEM and TEM analyses discussed before, the average particle size of the C-$LiFePO_4$ is ~200 nm and hence higher capacity is expected for lower current rate (≤C/2). However in our case, higher capacity was not achieved except for C/5 and this can be attributed to the agglomeration of particles as seen from the TEM results. Hence, by avoiding the agglomeration of the particle and by reducing the particle size, large fraction of cathode can be made accessible for Li-ion (de)intercalation. In short, cathodes with particles in the nanometer scale shorten the Li^+ diffusion distances and minimize the tortuous transport; hence, less time is needed to achieve full charge or discharge at the same current density.

4. Conclusions

Pure $LiFePO_4$ and C-$LiFePO_4$ composite cathode materials were prepared by solid-state route. Carbon as an additive reduces particle growth and retards the Fe^{2+} to Fe^{3+} oxidation and thereby eliminates the formation of impurity phase during high-temperature calcination. TEM results indicate carbon coating on the surface of $LiFePO_4$ and micro-Raman analysis suggests carbon in the amorphous form. The structural stability and reversibility upon electrochemical cycling is verified with ex situ Raman scattering. In case of C-$LiFePO_4$, the Li ion diffusion coefficient was $\sim 7.13 \times 10^{-14}$ cm^2s^{-1} where as in the case pure $LiFePO_4$ it was merely $\sim 1.28 \times 10^{15}\,cm^2s^{-1}$, and hence, the Li ion (de)intercalation was better in C-$LiFePO_4$. Excellent cycleability (~97% retention after 50 cycles) was attained for C-$LiFePO_4$ compared to pure $LiFePO_4$ (only 69% retention after 25 cycles). As the C-rate is increased, the discharge capacities of $LiFePO_4$ and C-$LiFePO_4$ cathodes are reduced. The poor discharge capacity at high C-rate is thought to be due to lower Li-ion diffusion and hence the rate capability can be improved

by reducing the particle size and by avoiding agglomeration in C-$LiFePO_4$. This comparative study reveals the necessity of conductive coating along with particle size reduction for improving the electrochemical properties of $LiFePO_4$ at high C-rate.

Acknowledgments

The financial support from NASA-EPSCoR (NNX08AB12A) and NASA-URC (NNX08BA48A) Grants is gratefully acknowledged. Continual support from UPR materials characterization center (MCC) is also acknowledged. One of the authors (SBM) thanks Council of Scientific and Industrial Research, Government of India for partial financial support for this publication.

References

[1] A. K. Padhi, K. S. Nanjundaswamy, and J. B. Goodenough, "Phospho-olivines as positive-electrode materials for rechargeable lithium batteries," *Journal of the Electrochemical Society*, vol. 144, no. 4, pp. 1188–1194, 1997.

[2] A. S. Andersson and J. O. Thomas, "The source of first-cycle capacity loss in $LiFePO_4$," *Journal of Power Sources*, vol. 97-98, pp. 498–502, 2001.

[3] H.-C. Kang, D.-K. Jun, B. Jin, et al., "Optimized solid-state synthesis of $LiFePO_4$ cathode materials using ball-milling," *Journal of Power Sources*, vol. 179, no. 1, pp. 340–346, 2008.

[4] H. Huang, S.-C. Yin, and L. F. Nazar, "Approaching theoretical capacity of $LiFePO_4$ at room temperature at high rates," *Electrochemical and Solid-State Letters*, vol. 4, no. 10, pp. A170–A172, 2001.

[5] J. D. Wilcox, M. M. Doeff, M. Marcinek, and R. Kostecki, "Factors influencing the quality of carbon coatings on $LiFePO_4$," *Journal of the Electrochemical Society*, vol. 154, no. 5, pp. A389–A395, 2007.

[6] Z. Xu, L. Xu, Q. Lai, and X. Ji, "Microemulsion synthesis of $LiFePO_4$/C and its electrochemical properties as cathode materials for lithium-ion cells," *Materials Chemistry and Physics*, vol. 105, no. 1, pp. 80–85, 2007.

[7] J. Chen, S. Wang, and M. S. Whittingham, "Hydrothermal synthesis of cathode materials," *Journal of Power Sources*, vol. 174, no. 2, pp. 442–448, 2007.

[8] Y.-H. Huang, K.-S. Park, and J. B. Goodenough, "Improving lithium batteries by tethering carbon-coated $LiFePO_4$ to polypyrrole," *Journal of the Electrochemical Society*, vol. 153, no. 12, pp. A2282–A2286, 2006.

[9] Y.-N. Xu, S.-Y. Chung, J. T. Bloking, Y.-M. Chiang, and W. Y. Ching, "Electronic structure and electrical conductivity of undoped $LiFePO_4$," *Electrochemical and Solid-State Letters*, vol. 7, no. 6, pp. A131–A134, 2004.

[10] N. Ravet, Y. Chouinard, J. F. Magnan, S. Besner, M. Gauthier, and M. Armand, "Electroactivity of natural and synthetic triphylite," *Journal of Power Sources*, vol. 97-98, pp. 503–507, 2001.

[11] M. Gaberscek, R. Dominko, and J. Jamnik, "Is small particle size more important than carbon coating? An example study on $LiFePO_4$ cathodes," *Electrochemistry Communications*, vol. 9, no. 12, pp. 2778–2783, 2007.

[12] F. Croce, A. D'Epifanio, J. Hassoun, A. Deptula, T. Olczac, and B. Scrosati, "A novel concept for the synthesis of an improved $LiFePO_4$ lithium battery cathode," *Electrochemical and Solid-State Letters*, vol. 5, no. 3, pp. A47–A50, 2002.

[13] A. Caballero, M. Cruz-Yusta, J. Morales, J. Santos-Peña, and E. Rodríguez-Castellón, "A new and fast synthesis of nanosized $LiFePO_4$ electrode materials," *European Journal of Inorganic Chemistry*, no. 9, pp. 1758–1764, 2006.

[14] G. X. Wang, L. Yang, Y. Chen, J. Z. Wang, S. Bewlay, and H. K. Liu, "An investigation of polypyrrole-$LiFePO_4$ composite cathode materials for lithium-ion batteries," *Electrochimica Acta*, vol. 50, no. 24, pp. 4649–4654, 2005.

[15] S.-Y. Chung, J. T. Bloking, and Y.-M. Chiang, "Electronically conductive phospho-olivines as lithium storage electrodes," *Nature Materials*, vol. 1, no. 2, pp. 123–128, 2002.

[16] P. S. Herle, B. Ellis, N. Coombs, and L. F. Nazar, "Nano-network electronic conduction in iron and nickel olivine phosphates," *Nature Materials*, vol. 3, no. 3, pp. 147–152, 2004.

[17] M. S. Islam, D. J. Driscoll, C. A. J. Fisher, and P. R. Slater, "Atomic-scale investigation of defects, dopants, and lithium transport in the $LiFePO_4$ olivine-type battery material," *Chemistry of Materials*, vol. 17, no. 20, pp. 5085–5092, 2005.

[18] C. A. J. Fisher and M. S. Islam, "Surface structures and crystal morphologies of $LiFePO_4$: relevance to electrochemical behaviour," *Journal of Materials Chemistry*, vol. 18, no. 11, pp. 1209–1215, 2008.

[19] P. P. Prosini, M. Lisi, D. Zane, and M. Pasquali, "Determination of the chemical diffusion coefficient of lithium in $LiFePO_4$," *Solid State Ionics*, vol. 148, no. 1-2, pp. 45–51, 2002.

[20] H. Liu, C. Li, H. P. Zhang, L. J. Fu, Y. P. Wu, and H. Q. Wu, "Kinetic study on $LiFePO_4$/C nanocomposites synthesized by solid state technique," *Journal of Power Sources*, vol. 159, no. 1, pp. 717–720, 2006.

[21] S. B. Tang, M. O. Lai, and L. Lu, "Li-ion diffusion in highly (0 0 3) oriented $LiCoO_2$ thin film cathode prepared by pulsed laser deposition," *Journal of Alloys and Compounds*, vol. 449, no. 1-2, pp. 300–303, 2008.

[22] B. Ellis, P. S. Herle, Y.-H. Rho, et al., "Nanostructured materials for lithium-ion batteries: surface conductivity vs. bulk ion/electron transport," *Faraday Discussions*, vol. 134, pp. 119–141, 2007.

[23] K. Zaghib, A. Mauger, F. Gendron, and C. M. Julien, "Surface effects on the physical and electrochemical properties of thin $LiFePO_4$ particles," *Chemistry of Materials*, vol. 20, no. 2, pp. 462–469, 2008.

[24] Y. Wang, J. Wang, J. Yang, and Y. Nuli, "High-rate $LiFePO_4$ electrode material synthesized by a novel route from $FePO_4 \cdot 4H_2O$," *Advanced Functional Materials*, vol. 16, no. 16, pp. 2135–2140, 2006.

[25] J. J. Saavedra-Arias, N. K. Karan, D. K. Pradhan, et al., "Synthesis and electrochemical properties of $Li(Ni_{0.8}Co_{0.1}Mn_{0.1})O_2$ cathode material: Ex situ structural analysis by Raman scattering and X-ray diffraction at various stages of charge-discharge process," *Journal of Power Sources*, vol. 183, no. 2, pp. 761–765, 2008.

[26] N. K. Karan, J. J. Saavedra-Arias, D. K. Pradhan, et al., "Structural and electrochemical characterizations of solution derived $LiMn_{0.5}Ni_{0.5}O_2$ as positive electrode for Li-ion rechargeable batteries," *Electrochemical and Solid-State Letters*, vol. 11, no. 8, pp. A135–A139, 2008.

[27] M. Maccario, L. Croguennec, B. Desbat, M. Couzi, F. Le Cras, and L. Servant, "Raman and FTIR spectroscopy investigations of carbon-coated Li_xFePO_4 materials," *Journal of the Electrochemical Society*, vol. 155, no. 12, pp. A879–A886, 2008.

[28] A. Ait Salah, A. Mauger, K. Zaghib, et al., "Reduction Fe^{3+} of impurities in $LiFePO_4$ from pyrolysis of organic precursor

used for carbon deposition," *Journal of the Electrochemical Society*, vol. 153, no. 9, pp. A1692–A1701, 2006.

[29] C. M. Burba and R. Frech, "Raman and FTIR spectroscopic study of Li_xFePO_4 ($0 \leq x \leq 1$)," *Journal of the Electrochemical Society*, vol. 151, no. 7, pp. A1032–A1038, 2004.

[30] K. Dokko, S. Koizumi, K. Sharaishi, and K. Kanamura, "Electrochemical properties of $LiFePO_4$ prepared via hydrothermal route," *Journal of Power Sources*, vol. 165, no. 2, pp. 656–659, 2007.

[31] J. Rodríguez-Carvajal, "Fullprof-3.6 2006, program for Reitveld Refinement".

[32] N. Ravet, M. Gauthier, K. Zaghib, et al., "Mechanism of the Fe^{3+} reduction at low temperature for $LiFePO_4$ synthesis from a polymeric additive," *Chemistry of Materials*, vol. 19, no. 10, pp. 2595–2602, 2007.

[33] A. Kumar, R. Thomas, N. K. Karan, M. S. Tomar, and R. S. Katiyar, "Li-ion rechargeable batteries based on $LiFePO_4$: a comparative study on the nanostructured composite positive electrode with two different carbon coating," *ECS Transactions*, vol. 16, no. 29, pp. 143–149, 2009.

[34] D.-H. Kim and J. Kim, "Synthesis of $LiFePO_4$ nanoparticles in polyol medium and their electrochemical properties," *Electrochemical and Solid-State Letters*, vol. 9, no. 9, pp. A439–A442, 2006.

[35] C. M. Julien, K. Zaghib, A. Mauger, et al., "Characterization of the carbon coating onto $LiFePO_4$ particles used in lithium batteries," *Journal of Applied Physics*, vol. 100, no. 6, Article ID 063511, 7 pages, 2006.

[36] Y. Hu, M. M. Doeff, R. Kostecki, and R. Fiñones, "Electrochemical performance of sol-gel synthesized $LiFePO_4$ in lithium batteries," *Journal of the Electrochemical Society*, vol. 151, no. 8, pp. A1279–A1285, 2004.

[37] M. M. Doeff, Y. Hu, F. McLarnon, and R. Kostecki, "Effect of surface carbon structure on the electrochemical performance of $LiFePO_4$," *Electrochemical and Solid-State Letters*, vol. 6, no. 10, pp. A207–A209, 2003.

[38] T. Nakamura, Y. Miwa, M. Tabuchi, and Y. Yamada, "Structural and surface modifications of $LiFePO_4$ olivine particles and their electrochemical properties," *Journal of the Electrochemical Society*, vol. 153, no. 6, pp. A1108–A1114, 2006.

[39] P. Pasierb, S. Komornicki, M. Rokita, and M. Rękas, "Structural properties of Li_2CO_3-$BaCO_3$ system derived from IR and Raman spectroscopy," *Journal of Molecular Structure*, vol. 596, no. 1–3, pp. 151–156, 2001.

[40] J. Barker, M. Y. Saidi, and J. L. Swoyer, "Lithium iron(II) phospho-olivines prepared by a novel carbothermal reduction method," *Electrochemical and Solid-State Letters*, vol. 6, no. 3, pp. A53–A55, 2003.

[41] M. Takahashi, S.-I. Tobishima, K. Takei, and Y. Sakurai, "Reaction behavior of $LiFePO_4$ as a cathode material for rechargeable lithium batteries," *Solid State Ionics*, vol. 148, no. 3-4, pp. 283–289, 2002.

[42] D. Y. W. Yu, C. Fietzek, W. Weydanz, et al., "Study of $LiFePO_4$ by cyclic voltammetry," *Journal of the Electrochemical Society*, vol. 154, no. 4, pp. A253–A257, 2007.

[43] C. O. Avellaneda and L. O. S. Bulhões, "Intercalation in WO_3 and WO_3:Li films," *Solid State Ionics*, vol. 165, no. 1–4, pp. 59–64, 2003.

[44] J. Wang and J. M. Bell, "Kinetic behaviour of ion injection in WO_3 based films produced by sputter and sol-gel deposition—part II: diffusion coefficients," *Solar Energy Materials and Solar Cells*, vol. 58, no. 4, pp. 411–429, 1999.

[45] M. S. Mattsson, "Li insertion into WO_3: introduction of a new electrochemical analysis method and comparison with impedance spectroscopy and the galvanostatic intermittent titration technique," *Solid State Ionics*, vol. 131, no. 3, pp. 261–273, 2000.

[46] F. M. Michalak and J. R. Owen, "Parasitic currents in electrochromic devices," *Solid State Ionics*, vol. 86–88, part 2, pp. 965–970, 1996.

[47] C. G. Granqvist, *Handbook of Inorganic Electrochromic Materials*, Elsevier Science, Amsterdam, The Netherlands, 1995.

[48] M. Deepa, T. K. Saxena, D. P. Singh, K. N. Sood, and S. A. Agnihotry, "Spin coated versus dip coated electrochromic tungsten oxide films: structure, morphology, optical and electrochemical properties," *Electrochimica Acta*, vol. 51, no. 10, pp. 1974–1989, 2006.

[49] G. Leftheriotis, S. Papaefthimiou, and P. Yianoulis, "Dependence of the estimated diffusion coefficient of Li_xWO_3 films on the scan rate of cyclic voltammetry experiments," *Solid State Ionics*, vol. 178, no. 3-4, pp. 259–263, 2007.

[50] M. D. Levi and D. Aurbach, "The mechanism of lithium intercalation in graphite film electrodes in aprotic media:—part 1: high resolution slow scan rate cyclic voltammetric studies and modeling," *Journal of Electroanalytical Chemistry*, vol. 421, no. 1-2, pp. 79–88, 1997.

[51] M. D. Levi, Z. Lu, and D. Aurbach, "Application of finite-diffusion models for the interpretation of chronoamperometric and electrochemical impedance responses of thin lithium insertion V_2O_5 electrodes," *Solid State Ionics*, vol. 143, no. 3-4, pp. 309–318, 2001.

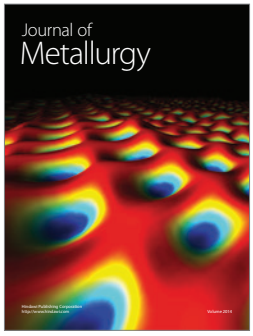

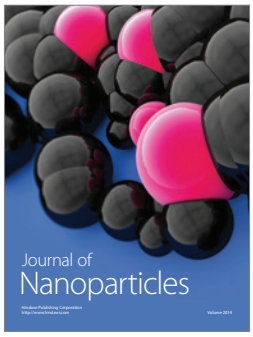

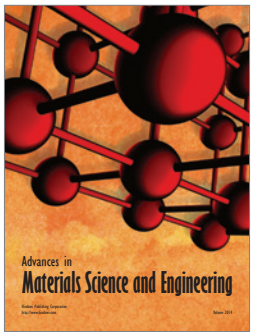

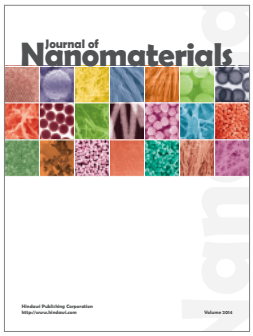

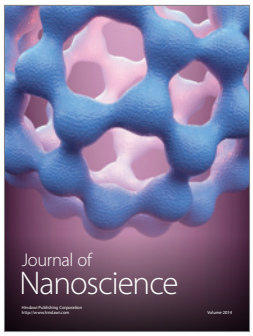

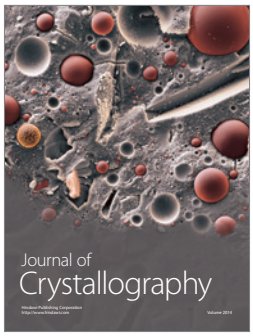

Hindawi

Submit your manuscripts at
http://www.hindawi.com